DOI: **10.1002/aenm.20180160510.1002/aenm.201801605**

New Generation Hole Transporting Materials for Perovskite Solar Cells: Non-Conjugated Small-Molecules

Michiel L. Petrus,[1] Kelly Schutt,[2] Maximilian T. Sirtl,[1] Eline M. Hutter,[3] Anna C. Closs,[1] James M. Ball,[4] Johan C. Bijleveld,[5] Annamaria Petrozza,[4] Thomas Bein,[1] Theo J. Dingemans,[6] Tom J. Savenije,[3] Henry Snaith,[2] and Pablo Docampo[7]**

[1] Department of Chemistry and Center for NanoScience (CeNS), University of Munich (LMU) Butenandtstr. 11, 81377 Munich, Germany

[2] Clarendon Laboratory, Department of Physics, University of Oxford, Parks Road, Oxford OX1 3PU, United Kingdom

[3] Opto-Electronic Materials Section, Department of Chemical Engineering, Delft University of Technology, van der Maasweg 9, 2629 HZ Delft, The Netherlands

[4] Center for Nano Science and Technology@Polimi, Istituto Italiano di Tecnologia, via, Giovanni Pascoli 70/3, 20133, Milan, Italy

[5] Delft University of Technology, Faculty of Aerospace Engineering, Kluyverweg 1, 2629 HS Delft, The Netherlands

[6] University of North Carolina, Department of Applied Sciences, 1112 Murray Hall Chapel Hill, NC 27599-3216, USA

[7] Newcastle University, School of Electrical and Electronic Engineering, NE1 7RU Newcastle upon Tyne, UK

e-mail: michiel.petrus@lmu.de; pablo.docampo@newcastle.ac.uk

Abstract

State-of-the-art perovskite-based solar cells employ an expensive, conjugated hole transporting material (HTM) such as Spiro-OMeTAD that, in turn, limits the commercialization of this promising technology. Herein we introduce an HTM (EDOT-Amide-TPA) with a functional amide-based backbone

which can be synthesized via a simple condensation reaction with an estimated cost of < $5 /gram. Moreover, unlike currently used HTMs, EDOT-Amide-TPA has a non-conjugated backbone, but still exhibits excellent charge transport properties indicating that intermolecular charge transport is key in this HTMs. When employed in perovskite solar cells, EDOT-Amide-TPA demonstrated stabilized power conversion efficiencies up to 20.0% and outperformed Spiro-OMeTAD. Moreover, the cells exhibit a longer lifetime, which is attributed to the coordination of the amide bond to the Li-additive. We show that non-conjugated materials can outperform state-of-the-art HTMs, thereby providing a novel set of design strategies to develop new, low-cost HTMs for realizing economically viable perovskite solar cells.

Hybrid metal halide perovskites have attracted enormous attention due to their simple preparation in combination with outstanding optoelectronic properties.[1] In 2009 these materials were introduced in solar cells and have since established a striking increase in performance, reaching over 22% in state-of-the-art devices.[2] Here, the perovskite absorber is sandwiched between two selective charge extraction layers, that transport the charges to the electrodes.[3] Although efficient inorganic hole transporting materials (HTMs) have been reported,[4] the most well-known HTMs are the organic materials 2,2',7,7'-tetrakis-(N,N-di-4-methoxyphenylamino)-9,9'-spirobifluorene (Spiro-OMeTAD) and polytriarylamine (PTAA). However, these materials are expensive, leading to a significant contribution to the total device cost.[5–7] The high cost arises from the multi-step synthesis, involving (transition) metal catalyzed cross-coupling reactions, stringent reaction conditions and extensive product purification. This tedious synthesis hampers large scale production of these materials and thereby could impede the commercial success of perovskite solar cells.

In contrast, our recently introduced approach using condensation chemistry, has proven its value as a low-cost and easily upscalable chemistry to prepare organic HTMs for perovskite solar cells.[8,9] Importantly, no expensive metal catalysts are required when using this chemistry, the synthesis can be done at ambient conditions and since water is the only side-product, the product purification is very straightforward.[10] Azomethine- and enamine-based organic molecules have been reported as HTMs, although none of these materials have been able to outperform state-of-the-art materials.[8,11,12]

Aromatic amides can also be synthesized using simple condensation chemistry and are well-known as building blocks for high-performance polymers with outstanding chemical and thermal stability. Kevlar is perhaps the most well-known example and owes its unique properties to a high backbone rigidity and strong intermolecular hydrogen bonding interactions. Nonetheless, as the amide-bond is not conjugated, it is generally believed to be a poor linker for the preparation of semiconducting materials, as it is postulated to hamper charge transport.[13] However, poor intramolecular charge transport may be overcome *via* enhanced intermolecular interactions in bulk materials. For instance, favorable hydrogen bonding can enforce close molecular packing and good intermolecular orbital overlap, and correspondingly enhanced charge transport properties.[14] For this reason we believe that aromatic amide-based HTMs have been overlooked and that their great potential remains untapped.

In this work, we introduce a simple HTM (EDOT-Amide-TPA) based on well-known building blocks, which are linked together with amide moieties. For a non-conjugated material this HTM shows outstanding charge carrier properties that can compete with conjugated state-of-the-art HTMs used in perovskite solar cells. Based on these results, we demonstrate that conjugation through the backbone is not essential in order to obtain materials with good charge transporting properties. The introduced amide-bond has the ability to coordinate with the Li-ions, and we hypothesis that this limits the migration of Li-containing additives, resulting in an improved device stability.[15] Using time-resolved microwave conductivity (TRMC) measurements, the charge transfer dynamics at the perovskite/HTM interface were

studied, revealing that our HTM efficiently extracts holes from the perovskite, and find that hole extraction by EDOT-Amide-TPA is faster than for Spiro-OMeTAD. We employed EDOT-Amide-TPA in perovskite solar cells and obtained devices with PCEs exceeding 20%. The performance, robustness and stability of these devices is compared with devices comprising current state-of-the-art material Spiro-OMeTAD. The amide-based material outperforms Spiro-OMeTAD in all categories at a twentieth of the cost, making this breakthrough a key development in the design of future low-cost HTMs.

Synthesis

The production of amide-based materials has proven its value in industry, as these materials can be made using straightforward chemistry with excellent yields and high purity. We use these aromatic amides as building blocks for the preparation of a semiconducting small-molecule termed "**EDOT-Amide-TPA"** (Figures 1a, S1 and S2), which was prepared by condensing 4-amino-4',4'',-dimethoxytriphenylamine (**3**) with 2,3-dihydrothieno[3,4-b][1,4]dioxine-5,7-dihydrochloric acid (**2**) in the presence of a base in a simple one-pot reaction. During the reaction the product precipitates, making the workup very straightforward, as only a simple washing step is required for purification. This results in a good isolated yield of 86% and very high purity, while the simplicity of the chemistry reduces batch-to-batch variations.

In order to give an estimate of the materials cost, we performed a cost-analysis following published procedures based on lab scale synthesis (Figure S3 and Table S1).[8,16] We obtained an estimated materials cost of only 5 $/gram, which is more than an order of magnitude lower than the estimated materials cost of Spiro-OMeTAD (92 $/gram) and also significantly lower than other high performing organic HTMs.[5,8,17,18] Additionally, EDOT-Amide-TPA can be synthesized without the use of halogenated solvents at only a slightly higher cost, which is essential for industrial production as many halogenated solvents have been banned from industrial processes.[19]

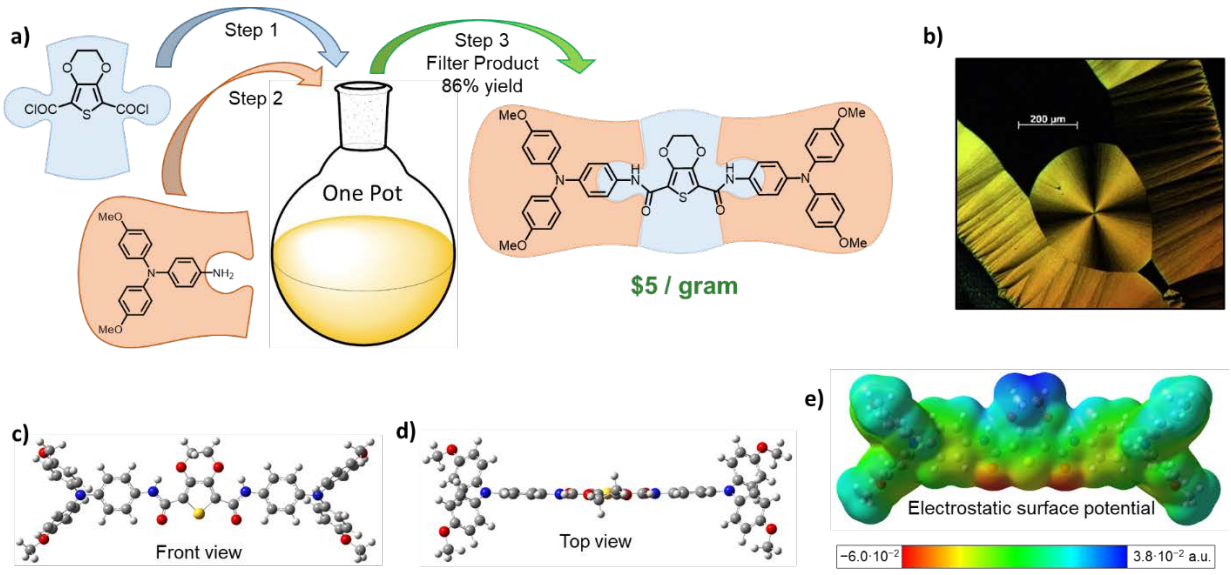

Figure 1 | **Structure of EDOT-Amide-TPA and its thermal properties**. **a**, One-pot reaction scheme and molecular structure of EDOT-Amide-TPA and its starting materials. **b**, Microphotographs (crossed polars 10x) of EDOT-Amide-TPA crystallized from the melt at 168 °C. **c** and **d**, Optimized geometry obtained from DFT calculation, displaying the planar core. **e**, Electrostatic surface potential map, revealing the strong dipole in the core.

Characterization

Aromatic amides are well-known for their outstanding thermal and chemical stability.[20] This is of importance for photovoltaic devices, as the HTM should not degrade under full operational conditions, which can reach over 80 °C. Thermogravimetric (TGA) measurements confirm the excellent thermal stability of the EDOT-Amide-TPA with a degradation temperatures close to 350 °C (Figure S4). Differential scanning calorimetry (DSC) measurements expose the polymorph character of EDOT-Amide-TPA (Figures 1b and S5), which was confirmed by X-ray diffraction measurements (Figure S6). The material has two different melting transitions, depending on the crystal structure, at 237 and 275 °C and a glass-transition temperature (T_g) at 112 °C, respectively. Additionally, a cold crystallization at 180 °C

was observed. All thermal transitions exceed the general operation temperature of photovoltaic devices and also the thermal transitions of its conjugated analogues (Table S2).

In order to estimate the bandgap of EDOT-Amide-TPA, light absorption measurements were performed (Figure 2a). The solvent has an influence on the absorption spectra, as protic and basic solvents can interact with the amide-bond. Comparable optical absorption spectra for chloroform solution and a thin film suggest that the EDOT-Amide-TPA film is in an amorphous state, which is in agreement with the lack of reflections in XRD measurements. The films show an absorption maximum at 395 nm and the absorption onset of the film was determined by a Tauc plot to be 485 nm, corresponding to an optical bandgap of 2.7 eV.

A good energy alignment between the perovskite absorber and the HTM is important to minimize losses in photovoltaic devices. The oxidation potential of EDOT-Amide-TPA was determined using cyclic voltammetry, from which the highest occupied molecular orbital (HOMO) energy level was calculated (Figure 2a, inset).[8] We observe a reversible oxidation with an onset at 0.53 V vs Ag/Ag^+, resulting in a HOMO energy level of −5.23 eV. The lowest unoccupied molecular orbital (LUMO) energy level was estimated to be −2.5 eV, obtained by adding the optical bandgap to the HOMO energy level. The HOMO energy level matches well with the valance band of the perovskite and is expected to result in minimal losses in the open-circuit voltage (V_{oc}), while the high LUMO energy level allows EDOT-Amide-TPA to function as an efficient electron blocking layer (Figure 2b).

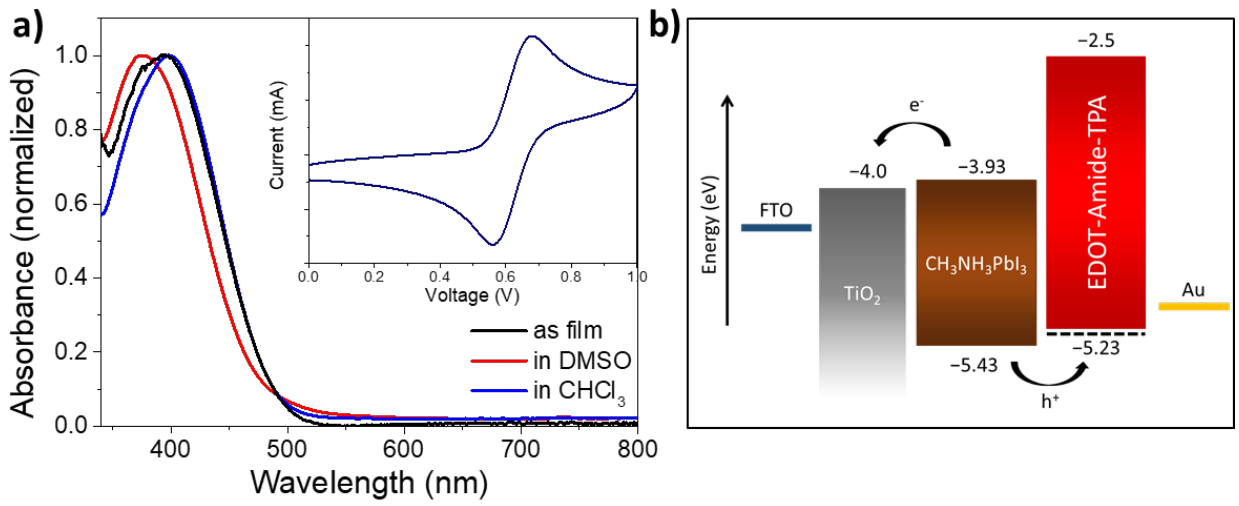

Figure 2 | **Optoelectronic properties of EDOT-Amide-TPA**. **a**, Normalized UV-Vis absorption profile of EDOT-Amide-TPA in chloroform, DMSO and as a thin film; the inset shows the cyclic voltammogram of EDOT-Amide-TPA measured in a dichloromethane solution containing $tBuNPF_6$ as electrolyte. Oxidation potential is measured vs. Ag/Ag^+. **b**, Energy level diagram showing the energy levels for EDOT-Amide-TPA obtained from cyclic voltammetry and UV-Vis measurements. The dotted line shows the HOMO energy level obtained from computational studies.

Molecular Geometry Simulations

Computational studies were performed to gain insight into the geometry and electronic structure of EDOT-Amide-TPA. Density functional theory (DFT) geometry optimizations were performed and the optimized geometry shows that the amide bond and the aromatic core of the molecule are all in a single plane, allowing for close molecular packing of the small-molecules (Figure 1c, d). The methoxy-containing phenyl rings of the triphenylamines are twisted out-of-plane, promoting the solubility of the small-molecule. The HOMO is concentrated over the triphenylamine side groups (Figure S7), while the LUMO is mostly located on the central thiophene moiety and the amide-bond. The HOMO energy level was theoretically estimated using the empirically obtained procedure published by Chi *et al.*,[21] and shows for EDOT-Amide-TPA a HOMO energy level of −5.30 eV, which is in excellent agreement with our experimentally obtained value.

The electrochemical surface potential (Figure 1e) reveals the electronegative character of the oxygens in the amide-bond, while the most electropositive part is located on the cyclic ether of the EDOT core, resulting in a dipole in the central moiety of the molecule. This dipole, combined with the amide-bond facilitating hydrogen bonding, is anticipated to enable a close molecular packing.[14]

Charge transport measurements

Although charge transport in small molecules relies on intermolecular charge transport, charge delocalization within the small molecules is generally considered important.[22] As the amide bond is not conjugated, materials with amide bonds in the backbone are generally believed to exhibit poor charge transporting properties in the bulk.[13] In order to study the potential of EDOT-Amide-TPA as a HTM for organic electronics, the charge transporting properties were thoroughly characterized.

For the hole mobility measurements, "hole-only" devices were prepared using the following device architecture: indium-doped tin oxide (ITO)/MoO_x/EDOT-Amide-TPA/MoO_x/Au.[23] *JV*-curves were recorded, with the current assumed to be space-charge limited at higher voltages (Figure S8). From this, the charge carrier mobility can be estimated using the Mott-Gurney equation.[23] The obtained mobility is $3.9 \cdot 10^{-5}$ $cm^2/(Vs)$ for EDOT-Amide-TPA, which is comparable to that Spiro-OMeTAD ($4.0 \cdot 10^{-5}$ $cm^2/(Vs)$). Upon addition of LiTFSI to the HTM, we observe a significant increase in the mobility to $2.1 \cdot 10^{-4}$ $cm^2/(Vs)$, which is ascribed to the reduction of the barrier height for charge hopping.[24]

The unexpectedly high hole mobility for EDOT-Amide-TPA was confirmed by using it as the active layer in bottom-gate, bottom-contact organic field effect transistors (OFETs, Figure S9). With this technique, the hole mobility for EDOT-Amide-TPA and Spiro-OMeTAD were found to be comparable, confirming the good charge carrier mobility for the non-conjugated EDOT-Amide-TPA.

Besides the charge carrier mobility, conductivity is an important measure for the charge transporting properties. We thus performed in-plane conductivity measurements (Figure 3a inset) with and without LiTFSI as additive. Upon increasing the concentration of LiTFSI in the HTM solution, the conductivity of EDOT-Amide-TPA increases spectacularly as shown in Figure 3a, reaching a value of $1.9 \cdot 10^{-3}$ S cm^{-1} when 300 mol% LiTFSI was added to the solution. We note that based on the area under the peaks in the optical absorption measurements, the amount of added LiTFSI does not directly correlate to the amount of oxidized species formed (Figure S12). In contrast, the conductivity in Spiro-OMeTAD has been reported to reach a maximum of $3 \cdot 10^{-5}$ S cm^{-1} upon addition of 20% LiTFSI, which is significantly lower.[25]

This thorough characterization of the charge transporting properties reveals that despite the anticipated poor intramolecular conjugation, EDOT-Amide-TPA shows excellent charge transporting properties that are at least as good as state-of-the-art reference materials such as Spiro-OMeTAD and its conjugated analogues (Table S3). This also indicates that intramolecular charge delocalization plays a minor role when it comes to facilitating bulk charge transport, which significantly broadens the horizon for the design of new HTMs.

Optical absorption measurements upon addition of LiTFSI reveal the formation of the oxidized species of the HTM (features at 700–800 nm), typical for most oxidized HTMs, and an additional shift of the original absorption peak around 400–440 nm (Figure 3b). The shift between the pristine film and the films containing LiTFSI is attributed to the coordination of the Li-ion to the amide-bond (inset Figure 3b), and was confirmed by infrared measurements (Figure S13). The coordination leads to an increased conjugation through the amide bond, explaining the observed red-shift. It is likely that besides catalyzing the formation of the oxidized species, the Li-coordination plays a role in the increased conductivity. Furthermore it increases the solubility of EDOT-Amide-TPA, thus enhancing the processability of the material. The improved solubility upon addition of lithium salts is well-known for amide-based materials

and originates from breaking up the intermolecular hydrogen bonds hence reducing the intermolecular interactions among neighboring molecules.[26–28]

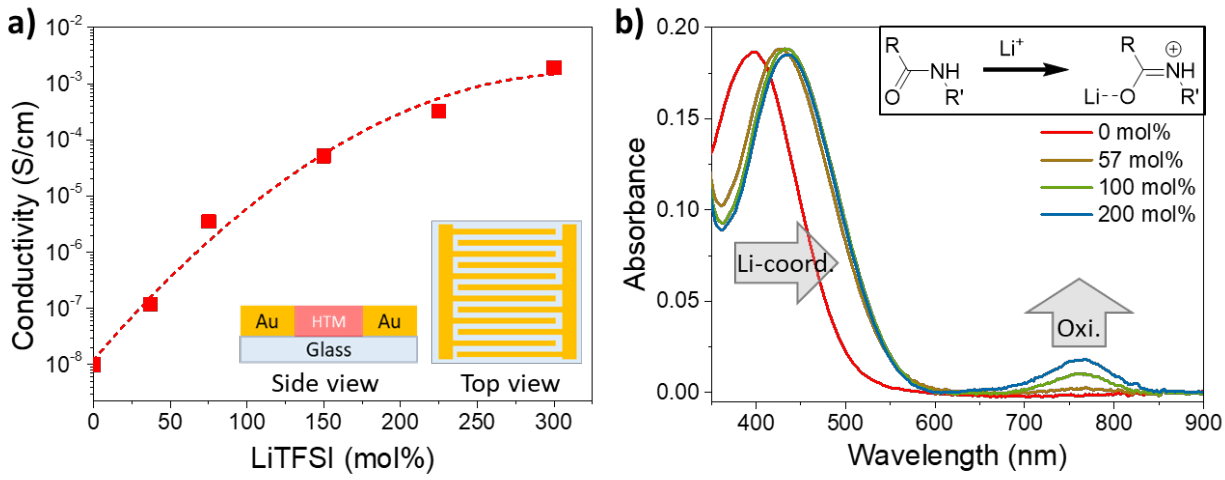

Figure 3 | **Charge transporting properties of EDOT-Amide-TPA**. **a**, The measured electrical conductivity as a function of the amount of LiTFSI added to the solution used for spincoating the films. The dotted line is added as a guide to the eye. The inset shows a schematic representation of the interdigitated electrode pattern on the device. **b**, UV-Vis absorption spectra of EDOT-Amide-TPA films as a function of added LiTFSI. The UV-vis spectra show the formation of the oxidized species in the range of 700–800 nm and a red-shift in the absorption maximum (400–440 nm) of the original species due to the coordination of the lithium-ions with the amide bond, as depicted in the inset.

Device Characterization

As high quality HTM films are required to obtain reproducible devices, the deposition of EDOT-Amide-TPA was optimized. Comparing films of EDOT-Amide-TPA and Spiro-OMeTAD shows that the Spiro-OMeTAD layers often has inhomogeneities (commonly referred to as asteroids) in the film, while this was significantly less apparent in the case of the EDOT-Amide-TPA films (Figure S14b).

The photovoltaic performance of EDOT-Amide-TPA as a charge extraction material was studied in planar methylammonium lead iodide ($MAPbI_3$) perovskite solar cells (fluorinated tin oxide (FTO)/compact TiO_2/$MAPbI_3$/EDOT-Amide-TPA/Au, Figure 4a). As perovskite photovoltaic cells often show significant batch-to-batch differences, several batches with a total of 128 individual devices were prepared to compare the photovoltaic performance between EDOT-Amide-TPA and Spiro-OMeTAD (Figures 4b, S10 and S11). This large dataset allows us to carefully compare the photovoltaic performance and to analyse the results using the t-test assuming unequal variance (Table S4). The statistical analysis shows that the increases in PCE, V_{oc} and J_{sc} are significant, while the increase in FF cannot be considered significant from this data set.

The higher open-circuit voltage is an especially important improvement, as it reaches up to 1.12 V for devices comprising EDOT-Amide-TPA, while devices with Spiro-OMeTAD did not exceed 1.08 V. We hypothesize that EDOT-Amide-TPA passivates the perovskite surface, hence reducing the interfacial recombination and thereby increasing the V_{oc}.[29] The high short-circuit currents also point to low interfacial recombination. Despite the significantly thinner HTM layer for EDOT-Amide-TPA (50 nm, Figure 4a) we find the distribution of PCE values to be narrower with this HTM, demonstrating the superior film forming properties of our material. The thinner HTM film has the additional advantage that it reduces the cost contribution of the HTM when employed in devices.

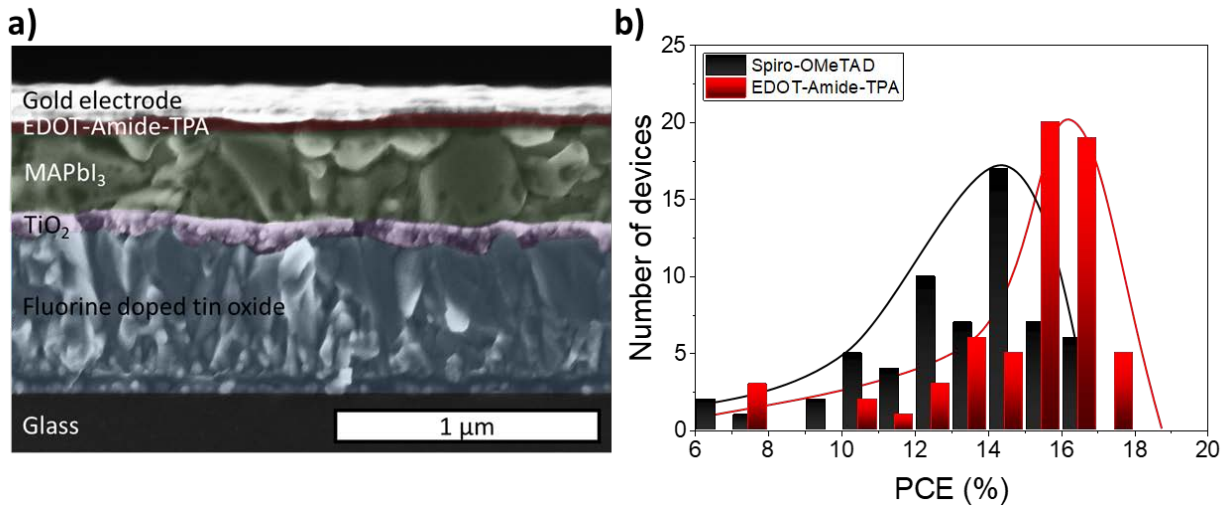

Figure 4 | **Photovoltaic performance of $MAPbI_3$ perovskite solar cells comprising EDOT-Amide-TPA and Spiro-OMeTAD as HTM**. **a**, SEM cross-section of full devices with the following architecture: FTO/compact TiO_2/$MAPbI_3$/EDOT-Amide-TPA/Au. **b**, Statistical evaluation of 128 individual devices prepared in different batches, comparing the power conversion efficiency of devices comprising either EDOT-Amide-TPA or Spiro-OMeTAD as HTM.

Recently, perovskites containing mixed halides and cations have been reported to outperform $MAPbI_3$ when applied in photovoltaic devices.[30] As these mixed-perovskites have been quickly adopted by the community, we additionally tested EDOT-Amide-TPA in combination with two of these state-of-the-art alternatives to $MAPbI_3$, namely: $(FA_{0.79}MA_{0.16}Cs_{0.05})Pb(I_{0.83}Br_{0.17})_3$ (FAMACs) and $FA_{0.83}Cs_{0.17}Pb(I_{0.83}Br_{0.17})_3$ (FACs). A significant improvement of the PCEs was also observed with these perovskites. In combination with FAMACs, PCEs up to 20.0% were obtained with EDOT-Amide-TPA and the V_{oc} reached up to 1.19 V, significantly outperforming Spiro-OMeTAD (Figures S14-17 and Tables S5-S6). The best photovoltaic performance was obtained with EDOT-Amide-TPA in combination with FACs serving as the perovskite absorber, showing a PCE of 20.3%; (V_{oc} = 1.16 V; J_{sc} = 22.7 mA/cm^2; FF = 77%), combined with a stunning stabilized power output of 20.0% (Figures 5a-b, S18-19 and Table S7). In contrast, the champion Spiro-OMeTAD reference device showed a PCE of 19.7% in the *JV*-scan with a stabilized power of 17.0%. The

external quantum efficiency spectrum is shown in Figure 5c and gives an integrated current of 21.4 mA cm^{-2}, which is in close agreement with the *JV*-scans. The PCE of 20.3%, obtained with EDOT-Amide-TPA as the HTM is among the highest reported PCEs for a (planar) perovskite solar cell using an alternative for Spiro-OMeTAD.[5,17,31,32] Furthermore, to the best of our knowledge, the stabilized power output of 20.0% is the highest reported efficiency for a device comprising $FA_{0.83}Cs_{0.17}Pb(I_{0.83}Br_{0.17})_3$ as absorber.[30,33,34] By exceeding literature values we have demonstrated that EDOT-Amide-TPA truly has the potential to outperform the current state-of-the-art HTMs in combination with different perovskite materials.

As shown in Figure 4b (Tables S4-S9), the use of EDOT-Amide-TPA is very robust, which we demonstrated by the enhanced performance in several individually prepared batches, using different perovskites. Additionally, we were able to reproduce these results in different labs, and across several batches of EDOT-Amide-TPA.

Excellent performance, low cost and high stability under operating conditions is essential for novel hole transporting materials. In order to study the stability, we tested devices without any encapsulation under accelerated aging conditions, and compared the performance of devices comprising EDOT-Amide-TPA with Spiro-OMeTAD. Aging was performed at open-circuit under an LED array (Figure S21), the temperature was controlled at 40 °C in a nitrogen atmosphere. The stabilized power output after 50 seconds was periodically measured, and is displayed in Figures 5d and S20.

Despite the substantially thinner hole transport layer, EDOT-Amide-TPA showed strikingly better stability than the devices comprising Spiro-OMeTAD. While the latter showed a pronounced loss in all photovoltaic parameters, no significant loss in the J_{sc} and FF was observed for devices comprising EDOT-Amide-TPA during the aging experiment (Figure S21-22 and Table S10). We believe that the outstanding stability of EDOT-Amide-TPA is related to the presence of the amide bonds, as the interactions between

the lithium-ions and the amide bonds likely facilitate a homogeneous distribution of the ions throughout the HTM layer and minimize their diffusion. In contrast, Lee *et al*. showed that in Spiro-OMeTAD layers LiTFSI accumulates at the perovskite interface, accelerating the degradation.[15] Degradation of the aged devices utilizing Spiro-OMeTAD is noticeable, where discoloration can be seen near the electrodes (Figure S23).

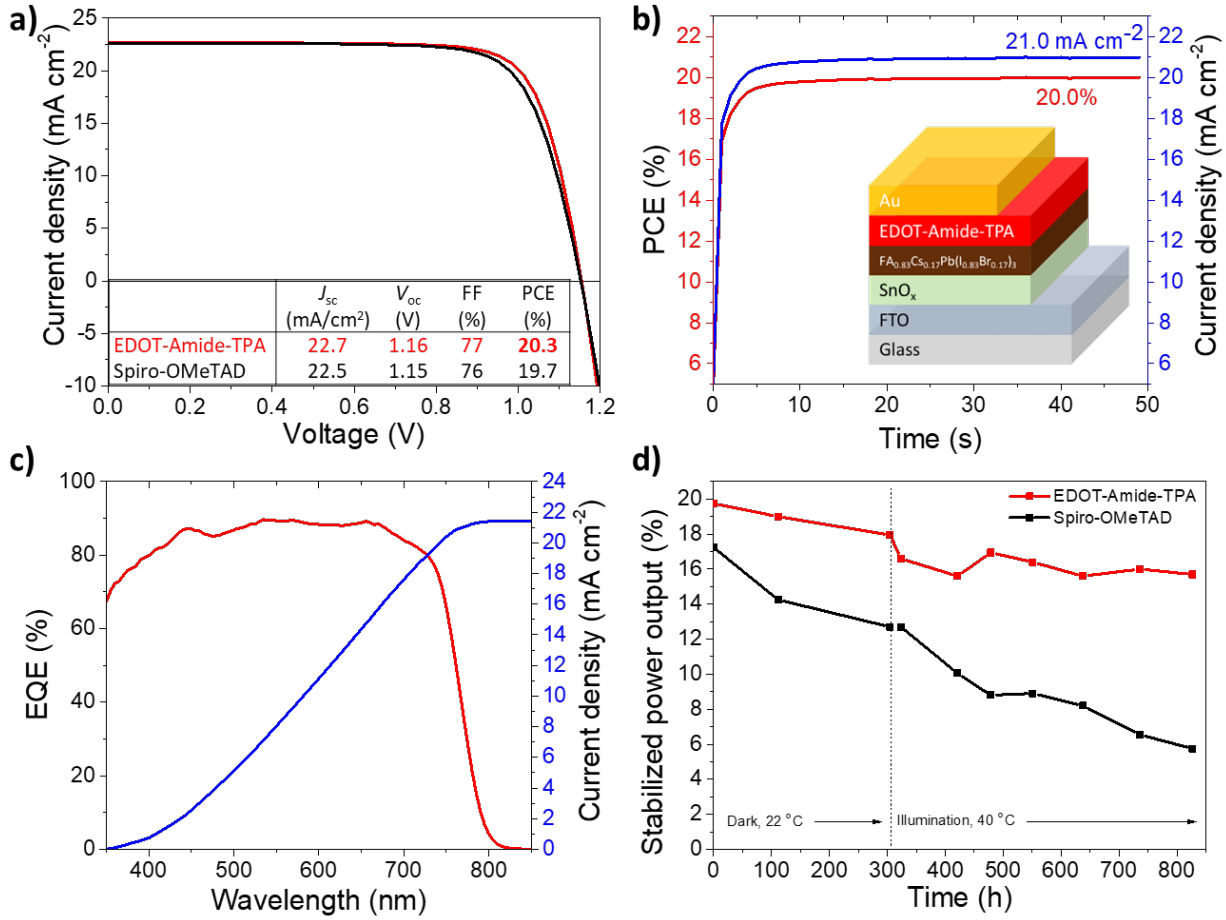

Figure 5 | **Photovoltaic performance and stability of $FA_{0.83}Cs_{0.17}Pb(I_{0.83}Br_{0.17})_3$ perovskite solar cells comprising EDOT-Amide-TPA or Spiro-OMeTAD as HTM. a**, *JV*-curves collected under AM 1.5 simulated sunlight of the champion devices comprising EDOT-Amide-TPA and Spiro-OMeTAD in the following device architecture: FTO/SnO_2/ $FA_{0.83}Cs_{0.17}Pb(I_{0.83}Br_{0.17})_3$/HTM/Au. The photovoltaic parameters are extracted from the *JV*-curves. **b**, Stabilized power output for the champion device comprising EDOT-Amide-TPA. **c**, External quantum efficiency with the

integrated current. **d**, Stabilized power output after aging the devices. Initial aging is performed in the dark, followed by testing under illumination at open-circuit at 40 °C. Cells were aged under nitrogen without encapsulation and periodically brought into atmosphere for measurements.

Time resolved microwave conductivity (TRMC)

To further investigate the origin of the outstanding performance of EDOT-Amide-TPA we used the TRMC technique, which has been shown to be a powerful technique to investigate the charge injection and recombination dynamics at the perovskite/charge transport layer interface.[35] With TRMC, we can measure the time-resolved photo-conductance and hence, get insight in the mobility and lifetimes of free charges.[36,37] Figure 6a shows the photo-conductance as function of time for a neat FAMACs film (blue) and bilayer films consisting of FAMACs combined with EDOT-Amide-TPA (red) or Spiro-OMeTAD (black) (more details can be found in the supporting information and Figure S24). The samples are excited at λ = 430 nm through the HTM, so that the majority of charge carriers in the perovskite layer is initially generated within 50 nm from the perovskite/HTM interface.[35] For the pure FAMACs film, the maximum signal height is close to 20 $cm^2/(Vs)$, representing the sum of electron and hole mobilities in the perovskite layer. For the bilayer samples, we note that if holes are extracted by the HTM, these do no longer significantly contribute to the signal as their mobility is only ~ 10^{-4} $cm^2/(Vs)$.[38] Therefore, the substantially reduced maximum signal height of 10 $cm^2/(Vs)$ in the FAMACs/EDOT-Amide-TPA bilayer shows that holes are extracted by the EDOT-Amide-TPA on a sub-ns timescale (*i.e.* faster than our instrumental response time).[38] Additionally, it suggests that both the electron and hole mobilities in these FAMACs perovskites are about 10 $cm^2/(Vs)$ and hence, highly balanced.[37] This is further confirmed by TRMC experiments in which we illuminated the sample (at λ = 430 nm) from the other side, thereby generating the charges several hundred nanometers away from the interface. As shown in Figure 6b, in the case of back side illumination, the sum of electron and hole mobilities is identical to the FAMACs

layer, indicating that no charge extraction has occurred on a sub-ns timescale. This can be understood considering that the holes first need to diffuse to the perovskite/EDOT-Amide-TPA interface before these can be extracted. Therefore, the above results show that EDOT-Amide-TPA extracts holes on a sub-ns timescale, provided that the holes are close to the interface. In contrast to the EDOT-Amide-TPA, the maximum signal height in the FAMACs/Spiro-OMeTAD bilayer is the same as for the pure FAMACs, even if charges are excited close to the interface (see Figure 6a and S25). From here, we conclude that extraction of holes from FAMACs by Spiro-OMeTAD is slower than by EDOT-Amide-TPA. The same behavior was observed using $MAPbI_3$ perovskites and is in agreement with PL quenching data (Figures S26-27), showing that the fast hole injection into EDOT-Amide-TPA is not unique to FAMACs perovskites. Fast injection into charge transport layers has been linked to a high J_{sc} in photovoltaic devices,[39,40] explaining the increase in the photocurrent observed for EDOT-Amide-TPA.

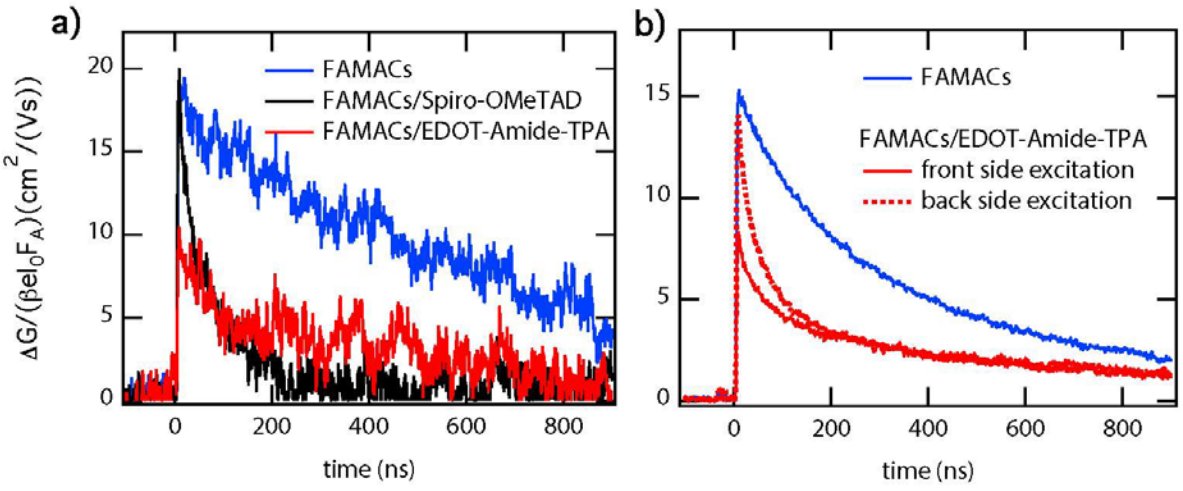

Figure 6 | **Time resolved microwave conductivity traces a.** for FAMACs (blue) and the bilayers FAMACs/EDOT-Amide-TPA (red) and FAMACs/Spiro-OMeTAD (black), recorded at 2 x 10^{10} absorbed photons/cm^2 (λ = 430 nm). **b.** for FAMACs (blue) and FAMACs/EDOT-Amide-TPA (red) illuminated through the HTM (front side, solid line) and through the perovskite (back side, dotted line), at 2 x 10^{11} absorbed photons/cm^2 (λ = 430 nm).

Discussion

What is the origin of the outstanding performance of non-conjugated EDOT-Amide-TPA serving as HTM in perovskite solar cells? In the following we offer a few possible explanations.

Charge transfer and interfacial recombination at the perovskite/HTM interface most likely plays a crucial role. Time-resolved microwave conductivity measurement performed on perovskite/EDOT-Amide-TPA bilayers show charge carrier lifetimes comparable to those of state-of-the-art materials.[35] However, the significantly lower signal amplitude observed for the perovskite/EDOT-Amide-TPA bilayer hints towards a faster hole injection rate, that has been linked to a high J_{sc} in photovoltaic devices.[39,40]

Several publications have shown that the perovskite surface can be passivated using a Lewis base, such as pyridine- or thiophene-based materials.[5,41,42] The amide moiety in EDOT-Amide-TPA also behaves like a Lewis base, and therefore a comparable interaction with the perovskite may be expected. This interaction is generally described as a passivation of iodine vacancies, whereby the Lewis base coordinates to the lead.[42] We hypothesize that this surface passivation enhances the effective charge transfer from the perovskite to the HTM and minimizes interfacial recombination.

The excellent performance might also be related to a more homogeneous distribution of the LiTFSI dopant throughout the HTM, facilitated by favorable Li-coordination to the amide moiety. When the additives accumulate at the perovskite/HTM interface, they are likely to increase charge recombination and thereby limit the V_{oc}.[15] The accumulation of Li-ions in Spiro-OMeTAD films will be significantly faster, as the ions can diffuse with minimal interaction within the hole transporting layer, leading to the fast degradation of the device.

Furthermore, we propose that a high quality thin HTM layer could play an important role in forming a good interface.[7] In this case the intermolecular interactions between the amide groups assist in the formation of high quality films. Further studies will be required to elucidate the origin of the fast hole injection, the enhanced device stability and the exact role of the amide bond as a functional backbone.

Conclusions

In summary, we have designed a novel non-conjugated small-molecule hole conductor, EDOT-Amide-TPA, that outperforms the state-of-the-art hole-transport material Spiro-OMeTAD when employed as the hole transporting layer in perovskite solar cells. PCEs of up to 20.3% were obtained with a stabilized power output of 20.0%. This stabilized power output is one of the highest reported efficiencies for HTMs in perovskite solar cells. The improved performance is the result of fast charge injection at the perovskite/EDOT-Amide-TPA interface, as was demonstrated by TRMC measurements. Photovoltaic devices comprising EDOT-Amide-TPA show excellent stability, which may be partially caused by the unique ability of the amide moiety to coordinate with LiTFSI. Here we establish that it is possible for non-conjugated small-molecules to feature charge transporting properties comparable to conjugated materials, indicating that intermolecular charge delocalization can play a dominant role when it comes to facilitating bulk charge transport behavior. Additionally, our material has the advantage that amides can be synthesized in a simple condensation reaction that is amenable to scale-up, leading to an estimated material cost of only 5 $/gram, while this chemistry can also be easily combined with a wide variety of other building blocks. To the best of our knowledge, this is the first demonstration of an HTM with a cost that is at least 10 times lower than Spiro-OMeTAD and that outperforms state-of-the-art HTMs. The combination of a significantly lower cost, better performance, higher reproducibility and improved stability makes EDOT-Amide-TPA an ideal candidate to replace Spiro-OMeTAD, and provides the community with a new set of design strategies to develop novel HTMs.

Methods

Synthesis of EDOT-Amide-TPA. General remarks. All chemicals were purchased from commercial sources and used as received unless stated otherwise. The synthesis was performed under nitrogen atmosphere. 4,4'-dimethoxy-4''-nitrotriphenylamine (**3**) was synthesized according to literature.[8]

*Synthesis of 3,4-Ethylenedioxythiophene-2,5-dicarbonyl chloride (**2**)*. 3,4-Ethylenedioxythiophene-2,5-dicarboxylic acid (**1**) (0.32 g; 1.36 mmol) was dissolved in tetrahydrofuran (THF; 20 mL) and dimethylformamide (DMF; 0.01 mL; 0.14 mmol) was added. Thionyl chloride ($SOCl_2$; 0.23 mL, 3.12 mmol) was added dropwise, resulting in a colour change to yellow. After heating the solution for 2 h. at 80 °C, the solution was allowed to cool down to R.T. and the remaining $SOCl_2$ and THF were removed under vacuum, resulting in the acid chloride **2** in a quantitative yield, which was used without further purification.

*Synthesis of N^5,N^7-bis(4-(bis(4-methoxyphenyl)amino)phenyl)-2,3-dihydrothieno[3,4-b][1,4]dioxine-5,7-dicarboxamide (**EDOT-Amide-TPA**)*. The total yield of the acid chloride **2** was dissolved in dry THF (20 mL) and 4-amino-4',4''-dimethoxytripehenylamine (**3**) (1 g; 3.12 mmol; 2.3 eq) was added followed by trimethylamine (0.1 mL) which was slowly added to the solution. The dark red solution was heated to reflux for 1.5 h resulting in a bright orange precipitate. The mixture was allowed to cool to R.T. overnight and the orange product was collected *via* filtration and washed with MeOH/Water and THF (yield = 0.99 g; 1.19 mmol; 86%). *^{1}H-NMR* **($CDCl_3$ + trimethylamine to prevent hydrogen bonding; 400 MHz): δ = 8.386 (s, 2 H), 7.396 (d_t, 4 H J = 9.2 Hz), 6.992 (d_t, 8 H, J = 9.2 Hz), 6.918 (d_t, 4 H, J = 8.8 Hz), 6.797 (d_t, 8 H, J = 9.2 Hz), 4.542 (s, 4 H), 3.785 (s, 12 H) ppm;** *^{13}C-NMR* **($CDCl_3$ + trimethylamine to prevent hydrogen bonding; 101 MHz): δ = 158.18, 155.74, 145.68, 141.24, 138.94, 130.87, 126.17, 121.89, 121.41, 119.16, 114.79, 65.46, 55.64 ppm;** *^{1}H-NMR* **(DMSO-d_6; 400 MHz): δ = 9.101 (s, 2 H), 7.487 (d_t, 4 H, J = 8.8 Hz), 6.966 (d_t, 8 H, J = 8.8 Hz), 6.891 (d_t, 8 H, J = 9.2 Hz), 6.816 (d_t, 4 H, J = 9.4 Hz), 4.537 (s, 4 H), 3.731 (s, 12 H) ppm;** *^{13}C-NMR* **(DMSO-d_6; 101 MHz): δ= 157.87, 155.33, 144.81, 140.53, 140.49, 131.07, 125.83, 121.62, 120.86, 116.28, 114.89, 65.33, 55.23 ppm;** *FTIR*: ν(cm^{-1}): 3373.9 (w), 2834 (vw), 1663 (m), 1600 (m), 1537 (m), 1501 (vs), 1462 (m), 1443 (w), 1372 (w), 1313 (s), 1285 (s), 1234 (vs), 1094(s), 1032 (m), 822 (s) 748 (m); *HRMS* (ESI^+): m/z calcd for $C_{48}H_{42}N_4O_8S^+$ $[M+H]^+$: 835.27961; found: 835.28076.

General characterization techniques. UV-Vis spectra were recorded using a Perkin Elmer Lambda 1050 spectrometer with an integrating sphere**.** FTIR were obtained using a Perkin Elmer FT-Infrared Spectrometer Paragon 1000. ^{1}H- and ^{13}C-NMRspectra were recorded using a Bruker spectrometer Avance III HD 400 MHz. All spectra where referenced to the solvent (^{1}H-NMR: $CDCl_3$ **δ = 7.26 ppm; DMSO-d6 = 2.50 ppm; ^{13}C-NMR:** $CDCl_3$ **δ = 77.0 ppm; DMSO-d6 = 39.51 ppm). HRMS measurements were carried out using a Thermo Finnigan LTQ FT Ultra.**

Cyclic voltammetry (CV). Cyclic voltammetry experiments were performed using a Metrohm Potentiostat (PGSTAT302N) with platinum working and counter electrode and an Ag/AgCl reference electrode. Experiments were performed in anhydrous and degassed dichloromethane solutions of the hole transporter with 0.1 M tetrabutylammonium hexafluorophosphate (tBuNPF6) as electrolyte and a scan rate of 100 mV s^{-1}. HOMO levels were calculated according to literature with the formal potential of the Fc^{+}/Fc redox positioned at −5.1 eV vs. vacuum.

Thermal characterization. Thermogravic analysis (TGA) was performed using a Netzsch STA 449 C Jupiter under nitrogen atmosphere with a scan rate of 10 °C min^{-1}. Differential scanning calorimetry (DSC) was performed under nitrogen atmosphere using a Perkin Elmer DSC8000 at a heating rates in the range of 10–50 °C min^{-1}. Melting behavior was confirmed using a melting point apparatus and Leica DMLM optical microscope equipped with crossed polars and a Linkham hot stage.

X-ray diffraction (XRD). X-ray diffraction analysis of HTM crystal structures was carried out in reflection mode using a Bruker D8 Discover diffractometer with Ni-filtered Cu $K\alpha_1$-radiation (λ = 1.5406 Å) and a position-sensitive semiconductor detector (LynxEye).

Preparation FACs and FAMACs devices:

Substrate etching and cleaning

All chemicals were purchased from Sigma Aldrich unless stated otherwise. Fluorine-doped tin oxide (FTO) coated glass substrates (Pilkington TEC 7) were patterned and then etched with 2 M HCl and zinc powder. Substrates were

scrubbed with detergent (2% Hellmanex in water) and then sequentially sonicated for 2 min in acetone, isopropyl alcohol, and nanopure deionized water. The FTO was treated in oxygen plasma for 10 min immediately prior to the spin-coating the electron transporting layer.

Tin oxide electron-transport layer

0.05 M tin (IV) chloride pentahydrate ($SnCl_4 \cdot 5H_2O$) was dissolved in 2-propanol and stirred for 30 minutes. The solution was spin-coated onto FTO at 3000 rpm for 30 s. Substrates were dried at 100 °C for 10 min and then annealed at 180 °C for 60 min. Substrates were then treated with a chemical bath deposition. 1.25 g urea was dissolved in 100 ml nanopure deionized water. 25 µL of 3-mercaptoproprionic acid (99%, Alfa Aesar) and 1.25 mL HCl (37%, Alfa Aesar) were added, and the solution was stirred vigorously for 2 min. The substrates were covered in the solution and placed in an oven at 70 °C for 3 h. Finally, the substrates were sonicated in deionized water for 2 min and then annealed again at 180 °C for 60 min. The substrates were treated with UV-ozone for 15 min immediately prior to perovskite deposition. All SnO_x-based devices contain 8 pixels per substrate.

FACs and FAMACs perovskite precursor solution and film deposition

1.45 M $FA_{0.83}Cs_{0.17}Pb(I_{0.83}Br_{0.17})_3$ precursor solution was prepared with 64 mg CsI (Alfa Aesar), 207 mg FAI (Dyesol), 538 mg PbI_2 (TCI), and 104 mg $PbBr_2$ (TCI). 1.5 M $Cs_{0.05}(FA_{0.83}MA_{0.17})_{0.95}Pb(I_{0.83}Br_{0.17})_3$ with excess lead iodide was prepared with 215 mg FAI, 28 mg MABr (Dyesol), 634 mg PbI_2, and 92 mg $PbBr_2$. A 1.875M solution of CsI in DMSO was then diluted into the precursor solution. Each perovskite solution was prepared in a mixture of anhydrous DMF (800 µL) and DMSO (200 µL). The precursor solution was stirred in atmosphere on a hot plate at 70 °C for 15 minutes. Room temperature precursor solution was deposited on FTO/SnO_2 substrates in a dry box and spin-coated at 1000 rpm for 10 s and then at 6000 rpm for 35 s (ramp of 2000 rpm s^{-1}). 80 µL of anisole was quickly dispensed onto the substrate 10 s before the end of spin-coating, and then the substrate was annealed on a hot plate at 100 °C for 45 min. The FACs perovskite was deposited at 8% relative humidity while the triple cation perovskite was deposited at 20% relative humidity.

Hole transport layer and electrode deposition FACs and FAMACs devices

The hole transport material (HTM) 2,2',7,7'-tetrakis(N,N'-di-p-methoxyphenylamine)-9,9'-spirobifluorene (spiro-OMeTAD) was prepared by dissolving 85 mg spiro-OMeTAD (Lumtec) in 1 ml anhydrous chlorobenzene along with 20 µl lithium bis(trifluoromethanesulfonyl)imide (Li-TFSI) salt in acetonitrile (500 mg ml^{-1}) and 33 µL tert-butylpyridine (tBP). 100 µl of spiro-OMeTAD solution was statically dispensed onto the substrate and then spin-coated at 2000 rpm for 45 s.

EDOT-Amide-TPA (EDOT) solution was prepared with 10 mg of EDOT in 800 µl anhydrous chlorobenzene and 200 µl chloroform along with 10 µl tBP and 20 µl Li-TFSI salt in acetonitrile (170 mg ml^{-1}). EDOT was heated at 105 °C for 5-10 minutes until the solution went transparent, and then passed through a 0.22 µm PTFE syringe filter while hot. The filtered solution was left on a hot plate at 85 °C while spin-coating. 50 µl EDOT solution was quickly dispensed onto the substrates while they were spinning at 1000 rpm for 40 s.

The substrates were left in a desiccator box for 48 h for the HTM to oxidize before thermally evaporating a 50 nm gold electrode under vacuum of < 7 x 10^{-6} torr.

FACs and FAMACs based solar cell characterization

Solar cells were measured with an Abet Class AAB solar simulator under simulated AM 1.5 sunlight at 100 mW cm^{-2} irradiance, calibrated by an NREL-calibrated KG5 filtered silicon reference cell. A spectral mismatch factor of 1.045 was estimated following a previously established protocol.[43] *JV*-curves were recorded with a 2400 Series Sourcemeter by Keithly Instruments. The solar cell were masked with a metal aperture with a defined active area of 0.0919 cm^{-2}. Stability measurements for FACs devices were performed in a nitrogen filled glovebox (H_2O and O_2 < 1 ppm) under an LED array, with devices held at 40 °C. The unencapsulated devices were periodically taken into atmosphere for 30 minutes for performance testing. The spectrum of the LED array was collected using a fibre-coupled Ocean Optics MAYAPro spectrometer with a cosine corrector attachment. The measured spectrum of the LED array is shown in Figure S19. No correction other than background subtraction has been applied to the measured spectrum.

Preparation $MAPbI_3$ devices:

Titanium oxide electron-transport-layer

2 M HCl (35 µL) in anhydrous 2-propanol (2.53 mL) was added dropwise to a solution of titanium isopropoxide (370 µL) in 2-propanol (2.53 mL) under vigorous stirring. The clear TiO_x sol-gel solution was spin-coated dynamically on the FTO substrates at 2000 rpm for 45 s, followed by annealing at 150 °C for 10 min on a hotplate. Finally, the TiO_2 compact layer, was completed by sintering at 500 °C in air for 45 min, resulting in a 20 nm thick TiO_2 compact layer and the substrates were cut into pieces of 3 × 3 cm^2. All TiO_x-based devices contain 12 pixels per substrate.

$MAPbI_3$ perovskite precursor solution and film deposition

For the $MAPbI_3$ precursor solution methylammonium iodide (Dyesol; 0.2 g; 1.25 mmol) and PbI_2 (TCI, >98%; 0.61 g; 1.3 mmol) were dissolved in *N,N*-dimethylformamide (DMF) : dimethyl sulfoxide (DMSO) solvent mixture (1:4 vol/vol; 1 mL) under stirring at 100 °C. The solution was spin-coated dynamically (80 µL; first at 1000 rpm for 10 s, followed by a second step at 5000 rpm for 30 s) onto the substrate. After 20 s, chlorobenzene (400 µL) was added on top of the spinning substrate and afterwards the substrate was annealed on a hotplate (first at 40 °C for 40 min, followed by a second step at 100 °C for 10 min).

Hole transport layer and electrode deposition $MAPbI_3$ devices

The hole transporting material spiro-OMeTAD (Borun Chemicals, 99.5% purity) was applied on the perovskite film using a 75 mg/mL solution in chlorobenzene. To this solutions 10 µL/mL 4-*tert*-butylpyridine (*t*BP) and 30 µl/mL of a 170 mg/mL bis(trifluoromethane)sulfonamide lithium salt (LiTFSI) solution in acetonitrile were added. For the optimized recipe, EDOT-Amide-TPA was dissolved at 10 mg/mL in a mixture of chlorobenzene : chloroform (4:1) to which 10 µL/mL *t*BP and 20 µl/mL of the LiTFSI was added at 75 °C (resulting in a clear orange solution). Spiro-OMetAD was spincoated dynamically at 1500 rpm while EDOT-Amide-TPA was spincoated at 1000 rpm both for 45 s. The devices were stored overnight under air at room temperature and < 30% RH to allow the hole transporting materials to oxidize. The top electrode with a thickness of 40 nm was deposited by thermal evaporation of gold under vacuum (at ~10^{-7} mbar).

$MAPbI_3$ based solar cell characterization. Current-Voltage (*JV*) characteristics of the perovskite solar cells were measured using a Newport OrielSol 2A solar simulator with a Keithley 2401 source meter. A spectral mismatch factor of 1.002 was estimated following a previously established protocol.[43] The devices were illuminated through a shadow mask, yielding an active area of 0.0813 cm^2. The *JV* curves were recorded under standard AM 1.5G illumination from a xenon lamp, calibrated to a light intensity of 100 mW cm^{-2} with a Fraunhofer ISE certified silicon diode. The input bias voltage was scanned from -1.5 V to 0 V in 0.05 V steps with a rate of 0.2 V s^{-1}. All prepared devices show a comparable degree of hysteresis between the forward and reverse scan.

External quantum efficiency measurements. External quantum efficiency (EQE) was measured via custom build Fourier transform photocurrent spectrometer based on a Bruker Vertex 80v Fourier Transform Interferometer. Devices were illuminated with an AM1.5 filtered solar simulator and calibrated with a Newport silicon reference diode with known external quantum efficiency. The devices were masked with a metal aperture with a defined active area of 0.0919 cm^2.

Charge transport measurements

Hole-only device preparation and characterization. ITO-substrates (1.5 x 2.0 cm, VisionTek, 12 Ω/sq to 15 Ω/sq) were etched and cleaned. The substrates were plasma cleaned prior to the thermal deposition of the MoO_x layer (10 nm) under vacuum (~$1 \cdot 10^{-6}$ mbar). The substrates were exposed to air and stored in a nitrogen-filled glovebox. Next, the EDOT-Amide-TPA was spincoated from chloroform at a concentration of 10 mg mL^{-1}, for the pristine materials and from a chlorobenzene:chloroform mixture as described above for the films in the presence of the additives. A top electrode of MoO_x (10 nm), followed by a layer of gold (40 nm) was deposited under vacuum ($1 \cdot 10^{-6}$ mbar). The active area of the device was 0.16 cm^2. Current-voltage characteristics were recorded in air in the dark using a Metrohm potentiostat (PGSTAT302N) at a scan rate of 0.1 V s^{-1}. The layer thickness which was around 50 nm was determined for the individual films by using atomic force microscopy (AFM) measurements, which were performed in tapping mode using a NanoInk DPN Stage microscope, or with a Veeco Dektak 150.

Organic field effect transistor (OFET) preparation and characterization. OFETs were prepared in a bottom-gate, bottom-contact geometry on n-doped Si wafers (serving as the substrate and gate electrode), coated with 230 nm

of thermally grown SiO_2 as the gate dielectric (C_i = 15 nF/cm^2), and photolithographically patterned interdigitated Au (30 nm thick, plus a 10 nm indium-doped tin oxide adhesion layer) source-drain electrodes (Fraunhofer IPMS). The substrates were cleaned sequentially in acetone and then isopropanol for 10 minutes each in an ultrasonic bath, followed by exposure to oxygen plasma for 10 minutes. The substrates were then immediately transferred to a nitrogen-filled glovebox for semiconductor deposition. EDOT-Amide-TPA thin-films were deposited by spincoating (speed = 2500 rpm, ramp = 2500 rpm/s, time = 45s) from a 10 mg/ml solution in chloroform. Spiro-OMeTAD thin-films were deposited by spincoating (speed = 2500 rpm, ramp = 2500 rpm/s, time = 45s) from a 10 mg/ml solution in chlorobenzene. The devices were then quickly transferred to a second glovebox in a parafilm-sealed box for electrical characterization using an Agilent B1500A semiconductor parameter analyzer. Optimal performance was obtained after annealing the devices at 180°C for 30 minutes in the glovebox.

Conductivity device preparation and characterization. Glass substrates with a thin compact layer of Al_2O_3 were used to improve the wetting of the HTMs on the substrate. EDOT-Amide-TPA was spincoated at 1000 rpm from chloroform solutions containing the given amount of LiTFSI as oxidant, resulting in a film thickness of approximately 50 nm. The films allowed to oxidize for 24 h in a desiccator at a relative humidity < 30%. 40 nm thick gold electrodes were thermally deposited under vacuum (~10^{-6} mbar). The electrode pattern was designed for two point probe measurements with a channel length of 250, 500 and 1000 µm, a channel width of 0.2, 0.1 and 0.056 m respectively. No significant differences were observed depending on the electrode pattern and the measured values were averaged over at least 8 individual devices. *JV*-curves were recorded under ambient conditions without illumination using a Keithley 2400 source meter at a scan rate of 1 V s^{-1} in the range from -5 to 5 V.

Time resolved microwave conductivity. The $MAPbI_3$ and FAMACs films with and without the HTM layer on top were spin-coated on quartz substrates using the same procedure as for the solar cell devices. The thin films on quartz substrates were placed in a sealed microwave cell inside an N_2-filled glovebox. The TRMC technique was used to measure the change in microwave (8.5 GHz) power after pulsed excitation (repetition rate 10 Hz) of the samples at different excitation wavelengths.[36] The bilayers were illuminated from the front side (through the HTM layer) or the back side. For bilayers comprising EDOT-Amide-TPA that have been excited through the HTM, the intensity has been corrected for the parasitic absorption of the HTM at 430 nm.

Computational study. The geometry optimization and electronic structure calculations were carried out using Gaussian09 program package. Density functional theory (DFT) geometry optimizations using the B3LYP/6-31G(d,p) basis set were performed in vacuum and in dichloromethane as the solvent, by means of the conductor-like polarizable continuum model (CPCM). The calculated HOMO energy level was obtained by adding 0.624 eV to the HOMO energy level obtained from DFT calculations using DCM as solvent.[21]

References

1 N. J. Jeon, J. H. Noh, Y. C. Kim, W. S. Yang, S. Ryu and S. Il Seok, *Nat. Mater.*, 2014, **13**, 897–903.

2 A. Kojima, K. Teshima, Y. Shirai and T. Miyasaka, *J. Am. Chem. Soc.*, 2009, **131**, 6050–6051.

3 M. L. Petrus, J. Schlipf, C. Li, T. P. Gujar, N. Giesbrecht, P. Müller-Buschbaum, M. Thelakkat, T. Bein, S. Hüttner and P. Docampo, *Adv. Energy Mater.*, 2017, **7**, 1700264.

4 N. Arora, M. I. Dar, A. Hinderhofer, N. Pellet, F. Schreiber, S. M. Zakeeruddin and M. Grätzel, *Science (80-.).*

5 M. Saliba, S. Orlandi, T. Matsui, S. Aghazada, M. Cavazzini, J.-P. Correa-Baena, P. Gao, R. Scopelliti, E. Mosconi, K.-H. Dahmen, F. De Angelis, A. Abate, A. Hagfeldt, G. Pozzi, M. Graetzel and M. K. Nazeeruddin, *Nat. Energy*, 2016, **1**, 15017.

6 A. Binek, M. L. Petrus, N. Huber, H. Bristow, Y. Hu, T. Bein and P. Docampo, *ACS Appl. Mater. Interfaces*, 2016, **8**, 12881–12886.

7 L. K. Ono, S. R. Raga, M. Remeika, A. J. Winchester, A. Gabe and Y. Qi, *J. Mater. Chem. A*, 2015, **3**, 15451–15456.

8 M. L. Petrus, T. Bein, T. J. Dingemans and P. Docampo, *J. Mater. Chem. A*, 2015, **3**, 12159–12162.

9 J. C. Hindson, B. Ulgut, R. H. Friend, N. C. Greenham, B. Norder, A. Kotlewski and T. J. Dingemans, *J. Mater. Chem.*, 2010, **20**, 937–944.

10 M. L. Petrus, R. K. M. Bouwer, U. Lafont, S. Athanasopoulos, N. C. Greenham and T. J. Dingemans, *J. Mater. Chem. A*, 2014, **2**, 9474–9477.

11 M. Daskeviciene, S. Paek, Z. Wang, T. Malinauskas, G. Jokubauskaite, K. Rakstys, K. T. Cho, A. Magomedov, V. Jankauskas, S. Ahmad, H. J. Snaith, V. Getautis and M. K. Nazeeruddin, *Nano Energy*, 2017, **32**, 551–557.

12 M. L. Petrus, A. Music, A. C. Closs, J. C. Bijleveld, M. T. Sirtl, Y. Hu, T. J. Dingemans, T. Bein and P. Docampo, *J. Mater. Chem. A*, 2017, **5**, 25200–25210.

13 C. R. Kemnitz and M. J. Loewen, *J. Am. Chem. Soc.*, 2007, **129**, 2521–2528.

14 I. Paraschiv, K. de Lange, M. Giesbers, B. van Lagen, F. C. Grozema, R. D. Abellon, L. D. A. Siebbeles, E. J. R. Sudholter, H. Zuilhof and A. T. M. Marcelis, *J. Mater. Chem.*, 2008, **18**, 5475–5481.

15 I. Lee, J. H. Yun, H. J. Son and T.-S. Kim, *ACS Appl. Mater. Interfaces*, 2017, **9**, 7029–7035.

16 T. P. Osedach, T. L. Andrew and V. Bulović, *Energy Environ. Sci.*, 2013, **6**, 711–718.

17 T. Malinauskas, M. Saliba, T. Matsui, M. Daskeviciene, S. Urnikaite, P. Gratia, R. Send, H. Wonneberger, I. Bruder, M. Graetzel, V. Getautis and M. K. Nazeeruddin, *Energy Environ. Sci.*, 2016, **9**, 1681–1686.

18 F. Zhang, Z. Wang, H. Zhu, N. Pellet, J. Luo, C. Yi, X. Liu, H. Liu, S. Wang, X. Li, Y. Xiao, S. M. Zakeeruddin, D. Bi and M. Grätzel, *Nano Energy*, 2017, **41**, 469–475.

19 D. Prat, O. Pardigon, H.-W. Flemming, S. Letestu, V. Ducandas, P. Isnard, E. Guntrum, T. Senac, S. Ruisseau, P. Cruciani and P. Hosek, *Org. Process Res. Dev.*, 2013, **17**, 1517–1525.

20 J. M. García, F. C. García, F. Serna and J. L. de la Peña, *Prog. Polym. Sci.*, 2010, **35**, 623–686.

21 W.-J. Chi, Q.-S. Li and Z.-S. Li, *Nanoscale*, 2016, **8**, 6146–6154.

22 P. Liu, B. Xu, Y. Hua, M. Cheng, K. Aitola, K. Sveinbjörnsson, J. Zhang, G. Boschloo, L. Sun and L. Kloo, *J. Power Sources*, 2017, **344**, 11–14.

23 M. L. Petrus, F. S. F. Morgenstern, A. Sadhanala, R. H. Friend, N. C. Greenham and T. J. Dingemans, *Chem. Mater.*, 2015, **27**, 2990–2997.

24 H. J. Snaith and M. Grätzel, *Appl. Phys. Lett.*, 2006, **89**, 262114.

25 A. Abate, T. Leijtens, S. Pathak, J. Teuscher, R. Avolio, M. E. Errico, J. Kirkpatrik, J. M. Ball, P. Docampo, I. McPherson and H. J. Snaith, *Phys. Chem. Chem. Phys.*, 2013, **15**, 2572–2579.

26 F. C. Grozema, A. S. Best, L. van Eijck, J. Stride, G. J. Kearley, S. W. de Leeuw and S. J. Picken, *J. Phys. Chem. B*, 2005, **109**, 7705–7712.

27 D. Balasubramanian and R. Shaikh, *Biopolymers*, 1973, **12**, 1639–1650.

28 H. Sigel and R. B. Martin, *Chem. Rev.*, 1982, **82**, 385–426.

29 R. A. Belisle, P. Jain, R. Prasanna, T. Leijtens and M. D. McGehee, *ACS Energy Lett.*, 2016, **1**, 556–560.

30 M. Saliba, T. Matsui, J.-Y. Seo, K. Domanski, J.-P. Correa-Baena, N. Mohammad K., S. M. Zakeeruddin, W. Tress, A. Abate, A. Hagfeldt and M. Grätzel, *Energy Environ. Sci.*

31 B. Xu, J. Zhang, Y. Hua, P. Liu, L. Wang, C. Ruan, Y. Li, G. Boschloo, E. M. J. Johansson, L. Kloo, A. Hagfeldt, A. K.-Y. Jen and L. Sun, *Chem*, 2017, **2**, 676–687.

32 D. Bi, B. Xu, P. Gao, L. Sun, M. Grätzel and A. Hagfeldt, *Nano Energy*, 2016, **23**, 138–144.

33 Z. Wang, Q. Lin, F. P. Chmiel, N. Sakai, L. M. Herz and H. J. Snaith, *Nat. Energy*, 2017, **2**, 17135.

34 D. P. McMeekin, G. Sadoughi, W. Rehman, G. E. Eperon, M. Saliba, M. T. Hörantner, A. Haghighirad, N. Sakai, L. Korte, B. Rech, M. B. Johnston, L. M. Herz and H. J. Snaith, *Science*, 2016, **351**, 151–155.

35 E. M. Hutter, J.-J. Hofman, M. L. Petrus, M. Moes, R. D. Abellon, P. Docampo and T. J. Savenije, *Adv. Energy Mater.*, 2017, **7**, 1602349.

36 T. J. Savenije, A. J. Ferguson, N. Kopidakis and G. Rumbles, *J. Phys. Chem. C*, 2013, **117**, 24085–24103.

37 Y. Hu, E. M. Hutter, P. Rieder, I. Grill, J. Hanisch, M. F. Aygüler, A. G. Hufnagel, M. Handloser, T. Bein, A. Hartschuh, K. Tvingstedt, V. Dyakonov, A. Baumann, T. J. Savenije, M. L. Petrus and P. Docampo, *Adv. Energy Mater.*, , DOI:10.1002/aenm.201703057.

38 C. S. Ponseca, T. J. Savenije, M. Abdellah, K. Zheng, A. Yartsev, T. Pascher, T. Harlang, P. Chabera, T. Pullerits, A. Stepanov, J.-P. Wolf and V. Sundström, *J. Am. Chem. Soc.*, 2014, **136**, 5189–5192.

39 J. Jiménez-López, W. Cambarau, L. Cabau and E. Palomares, *Sci. Rep.*, 2017, **7**, 6101.

40 J. Zhang, B. Xu, L. Yang, C. Ruan, L. Wang, P. Liu, W. Zhang, N. Vlachopoulos, L. Kloo, G. Boschloo, L. Sun, A. Hagfeldt and E. M. J. Johansson, *Adv. Energy Mater.*, 2017, 1701209.

41 H. Zhang, L. Xue, J. Han, Y. Q. Fu, Y. Shen, Z. Zhang, Y. Li and M. Wang, *J. Mater. Chem. A*, 2016, **4**, 8724–8733.

42 B. Chaudhary, A. Kulkarni, A. K. Jena, M. Ikegami, Y. Udagawa, H. Kunugita, K. Ema and T. Miyasaka, *ChemSusChem*, 2017, **10**, 2473–2479.

43 H. J. Snaith, *Energy Environ. Sci.*, 2012, **5**, 6513–6520.

Acknowledgements

The authors acknowledge Dr. Steffen Schmidt for the SEM images. This project was financed by a grant from the Federal Ministry of Education and Research (BMBF) under the project ID 03SF0516B. The authors acknowledge funding from the Bavarian Collaborative Research Program “Solar Technologies Go Hybrid” (SolTech), the Center for NanoScience (CeNS), the DFG Excellence Cluster “Nanosystems Initiative Munich” (NIM) and the Netherlands Organization for Scientific Research (NWO).

Author contributions

Synthesis and cost analysis were performed by M.L.P. and M.S. solar cell preparation and characterization was done by M.L.P., K.S. and M.S. Charge transport measurements were performed by M.L.P., A.C.C. and J.M.B. E.M.H. and T.J.S. performed and analyzed the TRMC measurements. Thermal and crystal analysis were performed by M.L.P., J.C.B. and T.J.D. Design of the HTM, UV-vis measurements, DFT calculations and the design of the project were done by M.L.P. The project was supervised by A.P., H.S., T.B., and P.D. All authors contributed to the writing of the manuscript.

Additional information

Supplementary information is available online.

Conflicts of Interest

There are no conflicts to declare.